Published in final edited form as:
J Am Chem Soc. 2008 July 2; 130(26): 8471–8480. doi:10.1021/ja801406f.

Structural Studies of the Molybdenum Center of the Pathogenic R160Q Mutant of Human Sulfite Oxidase by Pulsed EPR Spectroscopy and ^{17}O and ^{33}S Labeling

Andrei V. Astashkin[†], **Kayunta Johnson-Winters**[†], **Eric L. Klein**[†], **Changjian Feng**[†,‡], **Heather L. Wilson**[§], **K. V. Rajagopalan**[§], **Arnold M. Raitsimring**[†], and **John H. Enemark**[†]
Department of Chemistry, 1306 E University Blvd, University of Arizona, Tucson, Arizona 86721-0041, and Department of Biochemistry, Box 3711, Duke University Medical Center, Durham, North Carolina 27710

Abstract

Electron paramagnetic resonance (EPR) investigation of the Mo(V) center of the pathogenic R160Q mutant of human sulfite oxidase (hSO) confirms the presence of three distinct species whose relative abundances depend upon pH. Species 1 is exclusively present at pH ≤ 6, and remains in significant amounts even at pH 8. Variable-frequency electron spin echo envelope modulation (ESEEM) studies of this species prepared with ^{33}S-labeled sulfite clearly show the presence of coordinated sulfate, as has previously been found for the "blocked" form of *Arabidopsis thaliana* at low pH (Astashkin, A. V.; Johnson-Winters, K.; Klein, E. L.; Byrne, R. S.; Hille, R.; Raitsimring, A. M.; Enemark, J. H. *J. Am. Chem. Soc.* **2007**, *129*, 14800). The ESEEM spectra of Species 1 prepared in ^{17}O-enriched water show both strongly and weakly magnetically coupled ^{17}O atoms that can be assigned to an equatorial sulfate ligand and the axial oxo ligand, respectively. The nuclear quadrupole interaction (*nqi*) of the axial oxo ligand is substantially stronger than those found for other oxo-Mo(V) centers studied previously. Additionally, pulsed electron–nuclear double resonance (ENDOR) measurements reveal a nearby weakly coupled exchangeable proton. The structure for Species 1 proposed from the pulsed EPR results using isotopic labeling is a six-coordinate Mo(V) center with an equatorial sulfate ligand that is hydrogen bonded to an exchangeable proton. Six-coordination is supported by the ^{17}O *nqi* parameters for the axial oxo group of the model compound, (dttd)Mo^{17}O(^{17}Otms), where H_2dttd = 2,3:8,9-dibenzo-1,4,7,10-tetrathiadecane; tms = trimethylsilyl. Reduction of R160Q to Mo(V) with Ti(III) gives primarily Species 2, another low pH form, whereas reduction with sulfite at higher pH values gives a mixture of Species 1 and 2, as well as the "primary" high pH form of wild-type SO. The occurrence of significant amounts of the "sulfate-blocked" form of R160Q (Species 1) at physiological pH suggests that this species may be a contributing factor to the lethality of this mutation.

raj@biochem.duke.edu; jenemark@u.arizona.edu.
[†]University of Arizona.
[§]Duke University Medical Center.
[‡]Present address: College of Pharmacy, MSC09 5360, 1 University of New Mexico, Albuquerque, New Mexico 87131-0001.

Supporting Information Available: CW EPR spectra of R160Q SO reduced by Ti(III) citrate at pH 5.8; ^1H Re-Mims ENDOR spectra of Species 1 of R160Q SO; additional pulsed EPR data for (dttd)Mo^{17}O(^{17}Otms). This material is available free of charge via the Internet at http://pubs.acs.org.

Introduction

Sulfite oxidase (SO) catalyzes the oxidation of sulfite to sulfate as the terminal step in the metabolism of sulfur amino acids and is vital for human health. Inherited mutations in SO can result in severe neurological problems, stunted brain growth, and early death.[1] Investigation of the biochemistry of specific mutations has been greatly aided by the development of procedures for producing recombinant human sulfite oxidase (hSO). One of the most extensively studied clinical mutations that causes isolated sulfite oxidase deficiency is Arg 160 to Gln (R160Q),[2–4] which results from a single base change (guanine to adenine) in the gene for SO. No crystal structure is available for hSO, but the structure of the highly homologous chicken SO shows that R138 (equivalent to R160 in hSO) is in the active-site pocket near the Mo center which exhibits approximately square-pyramidal five-coordinate geometry in the fully oxidized Mo(VI) state, with axial and equatorial oxo ligands and three equatorial sulfur ligands (two from the pyranopterindithiolate cofactor and one from a cysteinyl side chain).[5] In the first step of the proposed catalytic cycle (Scheme 1, **A**→**B**) the equatorial oxo ligand reacts with sulfite to form an enzyme–product complex in which sulfate is coordinated to Mo (IV). Replacement of the product (sulfate) by water or hydroxide (**B**→**C**) and subsequent one-electron oxidations (Mo(IV/V/VI)) and concomitant deprotonations (**C**→**D**→**A**) return the Mo center to the fully oxidized resting state.[6–8]

Previous steady-state kinetic studies of the R160Q hSO mutant showed a nearly 1000-fold decrease in $k_{cat}/K_m^{sulfite}$, which suggested that the positive charge on Arg 160 in hSO makes an important contribution to the binding of sulfite.[2] Flash photolysis studies of intramolecular electron transfer (IET) between the molybdenum and heme domains showed that IET was also reduced about 1000-fold in R160Q compared to wild-type hSO. IET activity was partially restored in the R160K mutant, which has a positively charged lysine residue rather than the neutral glutamine of the fatal R160Q mutant.[9]

The crystal structure of the molybdenum domain of chicken R138Q shows that this mutation considerably reduces the size of the binding pocket and changes its overall geometry.[10] These findings suggest that steric factors, in addition to a change in the electrostatic potential at the active site, may play a role in attenuation of activity in the R160Q mutant. Similar ideas were entertained to explain different affinities of the Mo center to nitrate and sulfate in a related molybdenum enzyme, nitrate reductase.[11,12] To complicate the situation, a recent EXAFS investigation of the human R160Q mutant of SO suggested that, in R160Q, the glutamine 160 coordinates to the (sixth) axial position of the Mo center, *trans* to the oxo ligand.[13] However, no correlation between the proposed structural modification and the pathological consequences was explicitly discussed in that study.

EPR is a sensitive probe of Mo(V) and has long been used to study sulfite-oxidizing enzymes (SOEs). The continuous wave (CW) EPR spectra show significant differences among organisms, with pH, anions in the media and mutation of nearby amino acid residues, even though all available X-ray crystal structures reveal that the coordination geometries and structures of their Mo centers are essentially conserved.[5,14,15] The application of variable-frequency pulsed EPR techniques allows these qualitative observations to be rationalized in terms of local structural variations at the Mo(V) center.[16] Importantly, the differences between the principal *g*-values of most of the Mo(V) species formed in SO under various conditions are sufficiently large that, even in the microwave (mw) X-band, the individual SO forms present in a mixture can be studied selectively.[17] In addition, pulsed EPR is extremely useful for detecting the protons in the coordination environment of Mo(V). These protons are invisible to X-ray crystallography and EXAFS, but important for understanding the detailed mechanism of SO and its mutants. Finally, enrichment with magnetic isotopes (e.g. ^{17}O, $I = \frac{5}{2}$; ^{33}S, $I = \frac{3}{2}$) can be used to probe specific features of the Mo(V) forms of Scheme 1.

Recently we carried out detailed pulsed EPR studies of the structure of the Mo(V) forms of plant SO from *Arabidopsis thaliana* (At-SO).[6,18] These studies unambiguously demonstrated that reduction by sulfite at low pH resulted in a "blocked" form of the enzyme in which sulfate, the product, remained bound to Mo(V).[6] This "blocked" form is analogous to the phosphate- and arsenate-bound species of vertebrate SO.[19,20] This result for At-SO raised the question as to whether "blocked" forms also occur for hSO, particularly for mutants that show greatly reduced catalytic activity. Here we present a pulsed EPR investigation of the Mo(V) center of R160Q hSO. Both ^{17}O- and ^{33}S labeling have been used to gain insight into the structures that are adopted by R160Q. Our results confirm that at least three different Mo(V) species of R160Q exist as a function of pH, as found recently by Doonan et al.[13] We show that a "blocked" form with bound sulfate (Scheme 1, Species 1) is the only species at pH ≤ 6 and remains a significant form at physiological pH. This form represents a catalytic dead end, and we propose that it contributes to the lethality of the R160Q mutation. Additionally, the comparison of the hyperfine (*hfi*) and nuclear quadrupole interactions (*nqi*) of the oxo-^{17}O ligand with those known for other forms of SO and model oxo-Mo(V) complexes support the hypothesis that Species 1 of R160Q SO is six-coordinate.

Materials and Methods

Enzyme Preparation

Recombinant R160Q hSO was expressed and purified as previously described.[21] The EPR spectra of the low pH (*lpH*) (pH 5.8–6.0) forms of R160Q were obtained using sample buffers of 50 mM Bis-Tris propane. The enzyme was reduced with a 20-fold excess of sodium sulfite under argon and immediately frozen in liquid nitrogen. The same buffer system and procedure were used for reduction with ^{33}S-labeled sulfite, prepared as previously described.[6] The *lpH* form of R160Q in $H_2{}^{17}O$-enriched water was prepared by first concentrating a 200 μL solution of the enzyme in 25 mM Bicine and 25 mM Pipes at pH 6.2 to reduce the amount of $H_2{}^{16}O$. Next, a solution of 25 mM Bicine and 25 mM Pipes buffer was vacuum centrifuged to evaporate the $H_2{}^{16}O$, and the pelleted buffer was redissolved in the same volume of $H_2{}^{17}O$. The concentrated enzyme sample was then incubated in 30 μL of the buffer prepared with $H_2{}^{17}O$ for approximately 3 hat 4 °C. Finally, the enzyme was reduced with a 20-fold of excess sodium sulfite under argon, and the samples were immediately frozen in liquid nitrogen. Exchange into D_2O was accomplished by concentrating the protein samples to approximately 10 μL and then diluting them to ~300 μL with the appropriate buffer in D_2O. The procedure was repeated two times. The value of pD was calculated as $pD_{true} = pD_{apparent} + 0.4$.[22] For Ti(III) citrate-reduced *lpH* samples of R160Q in H_2O or D_2O, a stock solution of Ti(III) citrate was diluted to ~3.76 mM in 100 mM Bis-Tris propane (pH 6.0). Approximately 530 μM of R160Q in 50 mM Bis-Tris propane was injected into an EPR tube, which was then placed inside a Schlenk tube. The Schlenk tube was pumped to obtain mild vacuum and then purged with argon. This procedure was repeated several times over a period of 40 min to degas the protein. Next, 4 μL of the diluted Ti(III) citrate solution (250 μM final concentration) in well-degassed 100 mM Bis-Tris propane buffer (pH 6.0) was injected into the protein solution under Ar, and the reduced R160Q enzyme was frozen in liquid nitrogen immediately. The final ratio of [R160Q SO]/[Ti(III) citrate] was approximately 2:1.

Model System Synthesis

(1) $Mo^{17}O_2(acac)_2$—This precursor was prepared following a slightly modified published procedure.[23] Na_2MoO_4 (84.2 mg, 0.409 mmol) was dissolved in 500 μL of $H_2{}^{17}O$ (80.9 atom %, Isotec). The solution was stirred for 15 h. Freshly distilled 2,4-pentanedione (148 μL, 1.47 mmol) was added directly to the rapidly stirring solution, followed immediately by 6.0 M HCl (~120 μL, prepared by diluting concentrated reagent grade HCl by 50% with $H_2{}^{17}O$ of the same isotope concentration as above) slowly and dropwise until the solution pH = 2, resulting

in the precipitation of the product. The reaction mixture was stirred for 24 h. The precipitate was filtered off, washed generously with water (natural abundance), pentane, and then Et_2O to give the desired product as a tan powder.

(2) (dttd)$Mo^{17}O_2$—$Mo^{17}O_2(acac)_2$ (25 mg, 0.076 mmol) was dissolved in 2.0 mL of MeOH. To this was added dropwise a solution of 2,3:8,9-dibenzo-1,4,7,10-tetrathiadecane (H_2dttd) (24 mg, 0.077 mmol) and *tert*-butyl hydroperoxide (15 μL, 6 M in decane) in 2.0 mL of CH_2Cl_2 while rapidly stirring. Stirring was continued for 1 h at room temperature after the addition was complete. The reaction mixture was then carefully heated to 40 °C until the volume was reduced to 0.75 mL. Pentane (3 mL) was added to the resulting orange-red solution, and the mixture was stirred for 5 h. The desired product recrystallized from the solution as an orange-red powder and was filtered off, washed with pentane, a minimal volume of 40% MeOH in Et_2O, and then Et_2O, and was then dried *in vacuo* (11 mg, 33%). Characterization for natural abundance (dttd)MoO_2 prepared by the same procedure: *m/z* (relative intensity) 438 (100, M^+). UV–vis (DMF) [λ_{max}, nm (ε, M^{-1} cm^{-1})]: 410 (5250). ^{1}H NMR ($CDCl_3$, 300 MHz): 7.06–7.58 (m, 8H), 3.40 (d, J = 10.8 Hz, 2H), 3.06 (d, J = 10.8 Hz, 2H) ppm. Anal. Calcd for $C_{14}H_{12}MoO_2S_4$: C, 38.53; H, 2.77; O, 7.33. Found: C, 38.69; H, 2.86; O, 7.16.

(3) (dttd)$Mo^{17}O(^{17}$Otms)—(dttd)$Mo^{17}O_2$ (10 mg, 0.022 mmol) was dissolved in 0.5 mL of CH_2Cl_2. To this was added a solution of trimethylsilylsulfide ($(tms)_2S$) (18 mg, 0.10 mmol, 21 μL) in 0.5 mL of CH_2Cl_2 while rapidly stirring. The reaction mixture was stirred for 12 h during which time its color slowly changed from orange-red to deep purple. The product was not isolated from the reaction mixture. Characterization for natural abundance (dttd)MoO(Otms) prepared by the same procedure: *m/z* (relative intensity) 511 (100, M^+). UV–vis (toluene) [λ_{max}, nm (relative intensity)]: 382 (100), 553 (30). CW-EPR (9.340 GHz, 298 K, 2.02 mW, 1.0 G ma): g_{iso} = 1.96, $a(^{95,97}Mo)$ = 44 G. Chart 1 shows a graphical representation of (dttd)$Mo^{17}O(^{17}$Otms).

EPR Measurements

The CW EPR experiments were performed on a Bruker ESP-300 X-band spectrometer at 77 K. The electron spin echo envelope modulation (ESEEM) and pulsed electron–nuclear double resonance (ENDOR) experiments were performed on home-built X/K_u-band (8–18 GHz)[24] and K_a-band (26–40 GHz)[24,25]-pulsed EPR spectrometers. The exact microwave (mw) frequencies, ν_{mw}, for specific experiments are indicated in the Figure legends. The measurement temperature in the pulsed experiments was about 20 K.

The numerical simulations were done using the SimBud software.[24] In these simulations the orientations of the hyperfine interaction (*hfi*) and nuclear quadrupole interaction (*nqi*) tensors with respect to the *g*-frame (*x*,*y*,*z*) were described by the sets of Euler angles (φ_h,θ_h,Ψ_h) and (φ_q,θ_q,Ψ_q), respectively. The angles φ_h, θ_h and Ψ_h describe three consecutive rotations of the *hfi* reference frame (1,2,3) from the original state, when it coincided with the *g*-frame (1 // *x*, 2 // *y*, 3 // *z*): (1) by an angle φ_h around axis 3, (2) by an angle θ_h around the new axis 2, and (3) by an angle Ψ_h around the new axis 3. For the *nqi* reference frame (*X*,*Y*,*Z*) similar definitions apply.

Experimental Results

1. EPR and ESE Field Sweep Spectra

The EPR spectra observed for R160Q SO recorded at different pHs are shown in Figure 1. Reduction by sulfite at low pH (pH 6) gives a single EPR spectrum, as shown by trace 1 in Figure 1. At higher pH (pH 7–9.5) the EPR spectra showed the presence of several species. In all cases these spectra could be decomposed into three distinct spectra shown by traces 1–3 in

Figure 2. For convenience, the forms of the Mo(V) active centers giving rise to these signals are denoted as Species 1–3, with the numbering corresponding to that in Figure 2. The principal *g*-values for these three Species are summarized in Table 1. For comparison, Table 1 also gives the principal *g*-values of the "primary" low- and high pH forms established previously by Bray et al. for wild-type chicken SO,[26–28] and those of the recently observed "blocked" (SO_4^{2-}-coordinated) form of At-SO.[6,18] The notation for the principal *g*-values follows the convention: $g_z \geq g_y \geq g_x$, as indicated in Figure 2 for Species 1.

From Table 1 it appears that Species 3 is similar to "primary" *hpH* SO. However, Species 1 and 2 are clearly different from all of the other forms. Their most striking difference is the unusually small value of g_x compared to the wild-type (*wt*) enzyme. These observations are in agreement with the results of another recent work on R160Q SO by Doonan et al.,[13] who also found three different EPR spectra that were denoted as low-pH type 1 and type 2, and high-pH. In contrast, *wt* hSO exhibits only two different Mo(V) EPR spectra as a function of pH, which are the "primary" low-pH and high-pH spectra.[29]

The CW-EPR spectra of Species 1 and 2 show no splittings from nearby exchangeable protons and thus cannot provide information about the nature of the exchangeable equatorial ligand in these forms. Our previous studies with other types of SO preparations have shown that two possibilities may be operative. One possibility is that a coordinated OH group is present in the equatorial plane of the Mo(V) center, but the O–H bond is at a large angle with the plane of Mo(V) d_{xy} orbital that carries the unpaired electron. As a result, the isotropic *hfi* for this exchangeable proton becomes close to zero. Under such conditions, the presence of the equatorial OH ligand is only evident from a slight broadening at the EPR turning points resulting mostly from the anisotropic *hfi*. However, this proton was readily detectable by ESEEM and pulsed ENDOR, and detailed spectroscopic information was obtained from these pulsed EPR measurements. In particular, the anisotropic *hfi* constant was found to be statically distributed in rather broad limits as a result of the presence of various orientations of the OH ligand relative to the Mo(V) center.[31] This situation occurs in *wt hpH* SO and SDH [see e.g., refs [32–34]] and may also be the case for R160Q SO. Another possibility is that, similar to sulfite-reduced *lpH* At-SO,[6] Species 1 and/or 2 represent a "blocked" form, with the equatorial ligand being SO_4^{2-} instead of –OH.

One experiment that can be used to address this dilemma is to reduce the enzyme directly to Mo(V) with Ti(III) citrate,[30] a one-electron reductant, rather than through a pathway involving two-electron reduction by sulfite followed by subsequent one-electron oxidation to Mo(V). For At-SO at low pH, reduction with Ti(III) citrate resulted in formation of the "primary" *lpH* form instead of the "blocked" sulfate-coordinated form that was observed for a sulfite-reduction pathway.[18] In the present case of R160Q SO, reduction by Ti(III) citrate at pH 7.0 resulted in formation of a pure signal of Species 2 (trace 4 in Figure 2). Since there was no sulfite in this sample, it is clear that Species 2 does not represent a sulfate-coordinated form and, most likely, has an OH group as an exchangeable ligand.

If the Ti(III) reduction was performed at still lower pH (pH ≤ 6), then the EPR signal was a mixture of those of Species 2 and the "primary" (*wt*-like) signal of *lpH* SO (see Supporting Information). The main purpose of this work is to characterize Species 1. The full characterization of Species 2 will be the subject of a separate investigation.

The fact that the reduction of Mo(VI) by means of Ti(III) does not result in formation of Species 1 implies that this species might well represent a sulfate-coordinated ("blocked") form of SO. In order to definitively prove this, high-resolution pulsed EPR experiments have been performed. These experiments have simultaneously addressed the nature of the exchangeable ligand and the general nuclear surroundings of the Mo(V) center. Specifically, the unusual

values of the components of the **g** tensor of Species 1 could be a reflection of some identifiable structural differences between Species 1 and other forms of SO.

2. ESEEM Experiments with ^{33}S-Enriched Samples

The "blocked" form can be easily identified by ESEEM experiments on a sample prepared with ^{33}S-enriched sulfite. In this way we have recently unequivocally shown that the Mo(V) center in At-SO at low pH is "blocked" with a coordinated sulfate ligand.[6] Similar experiments were performed in this work. The samples of R160Q SO reduced by ^{33}S-enriched sulfite (99% ^{33}S, $I = \frac{3}{2}$) will be denoted ^{33}S-R160Q SO, while those prepared using sulfite with the natural abundance of sulfur isotopes (94.93% ^{32}S, $I = 0$) will be denoted ^{32}S-R160Q SO.

In our previous work, we have discussed the choice of an optimal mw operational frequency, ν_{mw}, to facilitate the observation of ^{33}S ESEEM from the coordinated sulfate.[6] By using an analogy with the phosphate- and arsenate-coordinated Mo(V) centers of SO studied earlier,[19,20] we have estimated the *hfi* parameters expected for ^{33}S of coordinated sulfate and have shown that the optimal ν_{mw} for ESEEM experiments in such a system should be between 16 and 24 GHz. The resonance magnetic fields B_o corresponding to these mw frequencies provide for the Zeeman/*hfi* cancelation condition, $\nu_S \approx A/2$ (where ν_S is the Zeeman frequency of ^{33}S and A is the *hfi* constant), which results in the largest ESEEM amplitude. Since our spectrometers do not cover the range of ν_{mw} between 18 and 26 GHz, the actual experiments on ^{33}S-At-SO were performed at $\nu_{mw} \approx 29$ GHz (K_a-band) in order to provide the so-called weak interaction regime ($\nu_S > A/2$), which usually simplifies the qualitative analysis of the ESEEM spectra. Most of the experiments in this work were also performed at $\nu_{mw} \approx 29$ GHz. For comparison, we have also performed some of the measurements in K_u band (at $\nu_{mw} \approx 17$ GHz) and found that the ESEEM amplitudes in both mw bands are comparable.

As an example, Figure 3 shows K_a- and K_u-band two-pulse ESEEM spectra of Species 1 of ^{33}S-R160Q SO obtained at g_z. All of the lines observed in these spectra within the frequency window shown were missing in the case of ^{32}S-R160Q SO, which allows one to assign them to the interaction of Mo(V) with ^{33}S. The feature of interest in these spectra is the peak at 18 MHz that belongs to one of the interdoublet transitions ($|\pm 1/2\rangle \leftrightarrow |\pm 3/2\rangle$) of ^{33}S within the electron spin manifold where the Zeeman and hyperfine interactions approximately cancel each other. The frequency of this transition is:

$$\nu_{id} \approx e^2Qq/2h \quad (1)$$

and we can easily estimate the quadrupole coupling constant $e^2Qq/h \approx 36$ MHz, very similar to $e^2Qq/h \approx 40$ MHz found for ^{33}S-At-SO.[6]

Panels a, c, and e in Figure 4 show K_a-band hyperfine sublevel correlation (HYSCORE) spectra obtained for Species 1 of ^{33}S-R160Q SO at the EPR turning points. The correlation peaks seen in these spectra are absent for the sample of ^{32}S-R160Q SO, which makes their assignment to ^{33}S straightforward. While these spectra look very simple and similar to those of a system with $I = 1/2$, this similarity is actually superficial because ^{33}S has spin $I = 3/2$ and strong *nqi* ($e^2Qq/h >> \nu_S, A$). The theory for interpreting this kind of spectra was developed in our previous work.[6] According to that theory, the pairs of crosspeaks seen in HYSCORE spectra belong to $|1/2\rangle \leftrightarrow |-1/2\rangle$ transitions of ^{33}S within the $|\alpha\rangle$ and $|\beta\rangle$ electron spin manifolds. The frequencies of these transitions, ν_α and ν_β, are approximately equal to:

$$\nu_{\alpha,\beta} = c_{hq} \cdot (\nu_s \pm [A/2]) \quad (2)$$

where c_{hq} is a numerical factor that depends on the orientation of the magnetic field vector, $\mathbf{B_0}$, relative to the *nqi* principal axes frame.

The approximate positions of the correlation peaks in panels a, c, and e of Figure 4 are respectively (2.9, 8.6), (1.8, 8.1), and (7.9, 7.9) [MHz], which give the corresponding center frequencies $\nu_c = (\nu_\alpha + \nu_\beta)/2$ of 5.75, 4.95, and 7.9 MHz. At the same time, the Zeeman frequency of ^{33}Sis $\nu_S \approx 3.5$ MHz (varies from 3.47 MHz at the low-field EPR turning point to 3.56 MHz at the high-field turning point). From these positions the scaling factors $c_{hq} = \nu_c/\nu_S$ can be estimated as 1.66, 1.40, and 2.22, which give the estimates for the *hfi* constants $A \sim 3.4$, 4.5, and 0 MHz. The signs of the effective *hfi* constants are as yet undefined, and two possible sets of the *hfi* constants are shown in Table 2.

The preliminary simulations of two-pulse ESEEM spectra similar to those described in our previous work showed that the experimental ESEEM amplitude can only be reproduced with the *hfi* parameters close to those of Set I,[6] and therefore this set was used as a starting approximation in the HYSCORE simulations. Since the largest c_{hq} was obtained for g_x, and it was greater than 2, it was reasonable to assume that the direction of the *nqi* axis *Y* was approximately parallel to the axis of g_x, in which case the rhombicity of the *nqi* tensor could be estimated as $\eta \approx 0.2$ (see published expressions).[6]

As a result of the simulations, the following set of parameters was obtained: $a_{iso} = 2.1$ MHz; $\mathbf{T} = (-4.1, 2.5, 1.6)$ MHz; $(\varphi_h,\theta_h,\Psi_h) = (20°, 10°, 20°)$, $e^2Qq/h = 36$ MHz; $\eta = 0.2$; $(\varphi_q,\theta_q,\Psi_q) = (90°, 90°, 0°)$. The simulated spectra are shown in panels b, d, and f of Figure 4. These parameters are rather similar to those obtained earlier for ^{33}S-At-SO, and a nonzero isotropic *hfi* constant is within the limits estimated from known *hfi* parameters for ^{31}P in coordinated phosphate and ^{75}As in coordinated arsenate.[19,20] The main qualitative conclusion from the observed significant ^{33}S *hfi* (both isotropic and anisotropic) is that Species 1 of R160Q SO represents a “blocked” form, with sulfate coordinated to the Mo(V) center.

3. ^{1}H- and ^{2}H-Pulsed ENDOR Experiments

The pulsed ENDOR experiments on samples of Species 1 of R160Q SO prepared in H_2O and D_2O (at pH ≤ 6) have revealed the presence of an exchangeable proton in close proximity to the Mo center, but with *hfi* parameters that are quite different from those of the “primary” *hpH* and *lpH* forms. As an example, Figure 5 shows the ^{1}H refocused (Re) Mims ENDOR[35,36] spectra obtained as a difference between the normalized (by ESE signal amplitude) spectra recorded for the samples in H_2O and D_2O. For brevity, these spectra will be referred to as the difference ^{1}H ENDOR spectra. The original experimental spectra recorded for several EPR positions are shown in the Supporting Information.

The largest splitting of ~5 MHz is observed at g_y, which indicates that the closest distance to an exchangeable proton from the Mo(V) center is $R_{MoH} \approx 3$ Å (as estimated using the point-dipole approximation, with the spin population on Mo(V) of 0.85). Numerical simulations of the difference ^{1}H ENDOR spectra were performed under the assumption that the exchangeable proton of interest is responsible for the exterior features in all spectra, while the interior features are also contributed by more distant exchangeable protons. As a result of these simulations, the isotropic *hfi* constant, a_H, was found to be about zero, and the anisotropic *hfi* tensor was found to be rhombic, with the principal components $(T_{11}, T_{22}, T_{33}) \approx (-3.0, -1.9, 4.9)$ MHz. The orientation of the *hfi* tensor with respect to the *g*-frame was described by the Euler angles $(\varphi_h, \theta_h, \Psi_h) = (75°, 80°, 0°)$. The simulations with axial anisotropic *hfi* tensor did not produce satisfactory results.

Figure 6 shows ^{2}H Mims ENDOR[37] spectra for the sample prepared in D_2O. Deuterons have spin $I = 1$ and rather weak *nqi* that results in extra splittings in the ENDOR spectra (compared

to the $I = ½$ case of ^{1}H) which complicates their analysis. The situation is, however, mitigated by the facts that we have already obtained the *hfi* estimates from the difference ^{1}H ENDOR spectra, and that the *nqi* tensor of deuterons is close to axial ($\eta \approx 0$). Therefore, in the ^{2}H ENDOR simulations we have used the *hfi* parameters rescaled according to the ratio of ^{2}H and ^{1}H magnetic moments, and varied the quadrupole coupling constant, e^2Qq/h, and the orientation of the ^{2}H *nqi* axis with respect to the *g*-frame. A reasonable fit of the experimental spectra was obtained for $e^2Qq/h = 0.2$ MHz and $(\varphi_q, \theta_q, \Psi_q) = (30°, –45°, 0°)$, see Figure 6.

4. ESEEM Experiments with ^{17}O-Enriched Samples

The ESEEM experiments with samples prepared with water enriched with ^{17}O (denoted for brevity ^{17}O-R160Q SO) have revealed the presence of ^{17}O in both equatorial and axial (oxo) positions. As an example, Figure 7 shows a HYSCORE spectrum of ^{17}O-R160Q SO (Species 1) obtained at g_y. The (++) quadrant of this spectrum shows two off-diagonal lines centered at the Zeeman frequency of ^{17}O, $\nu_O \approx 6$ MHz. The splitting between these lines is about 5.5 MHz, which gives an estimate of the *hfi* constant similar to that observed earlier for the oxo-^{17}O in chicken SO[38] and a model oxo-molybdenum complex.[39]

The (+–) quadrant shows a pair of lines due to the equatorial ^{17}O ligand. The splitting between these lines is equal to $2\nu_O \approx 12$ MHz, and the center of the doublet is located at the frequency of about 9 MHz, which gives an estimate of the *hfi* constant $A \approx 18$ MHz. This *hfi* constant is significantly lower than the values for the *lpH*, *hpH*, and phosphate forms of *wt* chicken SO that have a hydroxyl ligand in the equatorial position.[40–44] The observation of the equatorial ^{17}O in the ESEEM spectra of Species 1 of ^{17}O-R160Q implies that both oxo ligands were exchanged with ^{17}O during incubation of the Mo(VI) form of the enzyme and before reduction with sulfite.

To determine the quadrupole coupling constant of the oxo-^{17}O, the τ-integrated four-pulse ESEEM has been used.[32,45] Previously we have successfully used this technique to obtain spectra of the sum combination line of the oxo-^{17}O that showed resolved splittings due to the weak ^{17}O *nqi*.[39] Figure 8 shows the sum combination line region of the τ-integrated four-pulse ESEEM spectrum of ^{17}O-R160Q SO obtained at g_z, where the quadrupole splitting of the sum combination line was the largest, $\Delta\nu_\sigma \approx 1.5$ MHz. From this splitting, the quadrupole coupling constant of the oxo-^{17}O can be estimated as $e^2Qq/h \approx 5$ MHz ($e^2Qq/h \approx (40/12) \times \Delta\nu_\sigma$, see the relevant theory elsewhere[39]). For comparison, the quadrupole coupling constant determined earlier for $[Mo^{17}O(SPh)_4]^-$,[39] and *hpH* chicken SO[16] was much smaller, $e^2Qq/h \approx 1.5$ MHz.

5. ESEEM Experiments with ^{17}O-Enriched Model Compound (dttd)Mo^{17}O(^{17}Otms)

In addition to R160Q SO, we have also performed integrated four-pulse ESEEM experiments on the synthetic model compound (dttd)Mo^{17}O(^{17}Otms) shown in Structure 1. The primary goal of these experiments was to obtain *hfi* and *nqi* parameters for an axial oxo ligand in a six-coordinate molecule, as discussed below. The (dttd)Mo^{17}O(^{17}Otms) is well suited for obtaining ^{17}O parameters because the other coordination sites of Mo(V) are occupied by sulfur atoms (94.93% ^{32}S, $I = 0$). The HYSCORE and 2D refocused primary (RP) ESEEM measurements did not reveal the interaction with the oxygen of the equatorial ^{17}Otms ligand. This may be caused by the insufficient ^{17}O enrichment (estimated ~10% from the ^{17}O modulation amplitude) in combination with the generally greater difficulty of observing a strongly coupled equatorial oxygen. The axial oxo-^{17}O was, however, readily observed. The HY-SCORE and RP ESEEM experiments have shown that the *hfi* constant for this oxygen is similar to that in SO and the model compound studied earlier (~5 MHz).[38,39] The four-pulse experiment has, however, revealed that the quadrupole coupling constant for this compound, $e^2Qq/h \approx 3$ MHz, is about twice that in *hpH* SO and in $[Mo^{17}O(SPh)_4]^-$. As an example, Figure 9 shows the integrated four-pulse ESEEM spectrum obtained at g_z, where the largest

quadrupolar splitting of the sum combination line is observed. Additional experimental data for this compound can be found in the Supporting Information.

Discussion

In the experiments with ^{33}S-R160Q SO we have established that Species 1 represents a "blocked" form of SO, with sulfate coordinated to the Mo center. Compared with the "blocked" form reported for At-SO, however, Species 1 of R160Q SO has a more rhombic *g*-factor and an exchangeable proton situated close to the Mo(V) center. The *nqi* of the oxo ligand in ^{17}O-R160Q SO has more than tripled from the values observed for the model oxomolybdenum complex $[Mo^{17}O(SPh)_4]^-$,[39] and *hpH* SO.[16] In contrast, the *hfi* of this ligand is approximately the same as in other systems studied so far. Possible structural reasons for these findings are discussed below.

The anisotropic *hfi* of the exchangeable proton, while weaker than that generally observed for the proton of an OH ligand,[33,34] has significant rhombicity. This rhombicity can only be explained by an off-axis interaction with a spin population other than that located on the Mo center. Such a situation arises, e.g., for the proton of the OH ligand that interacts both with the large spin population on Mo ($\rho_{Mo} \approx 0.85$) and with the small spin population delocalized to the OH ligand oxygen ($\rho_O \approx 0.05$). For R160Q SO such a model would be invalid because the exchangeable ligand of the Mo center is, as we established, a sulfate group. However, the rhombicity of the anisotropic *hfi* tensor of the proton in question can be explained by considering the possible hydrogen-bonding interactions. One possibility is a hydrogen bond to the oxygen atom of sulfate that is coordinated to the Mo center; a second possibility is a hydrogen bond to the axial oxo ligand.

The estimation of the anisotropic *hfi* for the first model (sp^3-hybrid valence orbitals of oxygen, Mo–O distance of ~2.2 Å and the O···H hydrogen bond length of ~1.7 Å, the angle between Mo–H and Mo–O ≈ 30°) results in an anisotropic *hfi* tensor **T** = (–2.9, –2, 4.9) MHz, in qualitative agreement with the experimental data, **T** = (–3.0, –1.9, 4.9). For the second model (Mo=O···H, $\rho_O \approx -0.05$)[39], an anisotropic *hfi* tensor similar to the experimental one can only be obtained at a bonding angle of ~30° from the Mo=O direction. Such an angle would indicate a significant change of the hybridization of the oxo ligand orbitals resulting in significant s-character of the oxygen orbital that forms a σ-bond with the Mo d_z^2 orbital. This essentially nonzero s-character would lead to a dramatic increase of the isotropic ^{17}O *hfi* constant. Since the experimental ^{17}O *hfi* constant is similar to that found for other systems,[38,39] we discard this model as implausible.

Let us now consider the *nqi* parameters of the ^{17}O oxo ligand. A single electron in a p-orbital of ^{17}O produces a *nqi* tensor with $e^2Qq/h \approx 20$ MHz (and two electrons on the same orbital will result in $e^2Qq/h \approx 40$ MHz); however, six electrons in three mutually perpendicular p-orbitals give $e^2Qq/h = 0$ MHz (the result of cubic symmetry). If each of these p-orbitals donates exactly the same electronic population to the bonding orbitals of the Mo(V), then the oxo-^{17}O *nqi* will still be zero. The fact that the experimental *nqi* is very small ($e^2Qq/h << 40$ MHz) indicates that the electronic donations from the p-orbitals of ^{17}O are almost perfectly balanced. Indeed, in the detailed study of the axially symmetric model complex, $[MoO(SPh)_4]^-$, it was found that $\delta p_x = \delta p_y = \delta p_z \pm 0.07$.[39]

Unless a significant change in geometry of the molybdenum coordination occurs in R160Q SO, the dramatic increase in the quadrupole coupling constant of its axial oxo ligand relative to other recently studied systems requires alternative explanations. One possibility is a modification of the oxo ligand valence orbitals through asymmetric hydrogen bonding. Such an interaction would destroy the delicate balance between the electric field gradients produced

by the p-orbitals of the oxo group. However, such a hydrogen-bonding possibility has already been viewed as unlikely in the above discussion of the weakly coupled exchangeable proton observed for R160Q SO.

Alternatively, the change in the oxo-^{17}O *nqi* could reflect a decrease or increase in the electronic donations from some of the oxygen orbitals without modification of their geometry. This purely electronic effect could be caused by the weak axial coordination of a sixth ligand to Mo(V), *trans* to the oxo ligand, in the R160Q protein. Coordination of a sixth ligand would involve the same Mo(V) orbitals used in coordination of the oxo ligand and may thereby change the electronic donation pattern from the oxo ligand, which in turn may result in a different oxo-^{17}O *nqi*. In the recent investigation of R160Q SO by XAS and EXAFS the hypothesis of a six-coordinate structure for its Mo center has been also employed.[13]

In order to validate the above considerations, we have performed ^{17}O ESEEM experiments on the model six-coordinate Mo(V) complex, (dttd)Mo^{17}O(^{17}Otms), which has a thioether sulfur donor *trans* to the terminal oxo ligand (Structure 1). The quadrupole coupling constant of the oxo-^{17}O determined for this compound is ~3 MHz, approximately twice that found for the oxo-^{17}O ligands in [Mo(V)^{17}O(SPh)$_4$]$^-$ and the Mo(V) center of *hpH* SO. This result demonstrates that axial coordination *trans* to the oxo-^{17}O produces an observable increase in the quadrupole coupling constant. In addition, the *nqi* for (dttd)-Mo^{17}O(^{17}Otms) provides strong, if indirect, support for the hypothesis that the increase of the quadrupole coupling constant of the oxo-^{17}O in Species 1 of R160Q SO (compared to the systems studied earlier) is caused by axial coordination *trans* to the oxo ligand, as proposed by Doonan et al.[13] Detailed quantum chemical calculations addressing the ^{17}O *hfi* and *nqi* parameters in (dttd)Mo^{17}O (^{17}Otms) and R160Q SO will be presented elsewhere.

Yet another factor, in addition to six-coordination, that could produce the unusual quadrupole coupling constants found for the oxo-^{17}O ligands of R160Q SO and (dttd)Mo^{17}O(^{17}Otms) are the equatorial ligands, which differ from those in previous enzyme and model systems. The change in the equatorial ligands can alter the electronic donation from the oxo ligand to d_{xz} and/or d_{yz} orbitals of the Mo(V) center, which could result in a different quadrupole coupling constant. However, the oxo-^{17}O *nqi* constants of [Mo(V)^{17}O(SPh)$_4$]$^-$ and the Mo(V) center of *hpH* SO are very similar even though their equatorial ligands are different. Likewise, the oxo-^{17}O *nqi* constants of the *lpH* and *hpH* forms of wt SO are similar even though the orientations of the OH ligand in the two forms of SO are different, which should result in different overlaps of the OH oxygen orbitals with the d_{xz} and d_{yz} orbitals of molybdenum. Therefore, while we cannot completely rule out the possibility that the change of the oxo-^{17}O *nqi* in R160Q SO is simply caused by the presence of a sulfate ligand, instead of a hydroxyl, in the coordination sphere of the Mo(V) center, the above examples make this explanation less plausible than that based on axial coordination. Further insight into these *nqi* variations will result from the detailed quantum chemical calculations on these systems that are in progress.

Conclusion

Three different paramagnetic species of R160Q SO can be generated, depending upon pH and the mode of reduction (Scheme 1). Species 1, which is the only one present at pH ≤ 6, is the primary focus of this report. Species 1 contains coordinated sulfate, as clearly demonstrated by ^{33}S ESEEM measurements. Moreover, the ^{33}S paramenters for Species 1 are similar to those previously found for the bound sulfate of the “blocked” form of At-SO.[6] Species 1 also has a nearby exchangeable proton that is likely to be hydrogen-bonded to an oxygen of the sulfate ligand. A proposed structure for the Mo(V) center of Species 1 in R160Q SO based on the experimental results obtained in this work and the above considerations regarding the oxo-^{17}O *nqi* is shown in Figure 10. The proposed weakly coordinated sixth ligand (X) that is *trans* to

the terminal oxo ligand is consistent with the larger oxo-^{17}O quadrupole coupling constant found for the known six-coordinate ^{17}O-labeled compound, (dttd)Mo^{17}O(^{17}Otms). Two possibilities for the *trans* ligand X (O or N) were discussed recently from EXAFS and DFT studies on R160Q SO.[13] From our studies, only X = O remains plausible because no ^{14}N modulations, which are easily detectable by ESEEM, were observed.

The structure of Figure 10 can be viewed as an enzyme–product complex that is trapped in the Mo(V) oxidation state, e.g. the hypothesized Mo(IV)-sulfate enzyme–product complex of Scheme 1 has been oxidized to Mo(V) *before* the substrate was hydrolyzed. As we already mentioned (see Figure 1), the fraction of Species 1 present decreases with increasing pH;[13] however, Species 1 remains a significant Mo(V) form at pH 7.2[13] and is still observable at pH 8.9. Thus, it is reasonable to speculate that the “blocked” structure of R160Q (Figure 10) represents a catalytic dead end that contributes to the lethality of this mutant under physiological conditions. The generation of “blocked” forms of SO, especially at low pH, appears to be an important feature in the biochemistry of other mutants of hSO, and the catalytically compromised Y343F mutant of hSO[17,47] also exhibits a “blocked” species with bound sulfate.[46]

Supplementary Material

Refer to Web version on PubMed Central for supplementary material.

Acknowledgments

We gratefully acknowledge support of this research by the NIH (GM-37773 to J.H.E., GM 44283 to K.V.R.) and by Grants from the NSF (DBI-0139459, DBI-9604939, BIR-9224431) and the NIH (S10RR020959) for development of the pulsed EPR facility. K.J.-W. thanks the NIH for a Ruth L. Kirschstein National Service Award.

References

1. Seidahmed MZ, Alyamani EA, Rashed MS, Saadallah AA, Abdelbasit OB, Shaheed MM, Rasheed A, Hamid FA, Sabry MA. Am. J. Med. Genet. Part A 2005;136A:205. [PubMed: 15952210]
2. Garrett RM, Johnson JL, Graf TN, Feigenbaum A, Rajagopalan KV. Proc. Natl. Acad. Sci. U.S.A 1998;95:6394. [PubMed: 9600976]
3. Johnson JL, Coyne KE, Garrett RM, Zabot M-T, Dorche C, Kisker C, Rajagopalan KV. Hum. Mutat 2002;20:74. [PubMed: 12112661]
4. Lam C-W, Li C-K, Lai C-K, Tong S-F, Chan K-Y, Ng GS-F, Yuen Y-P, Cheng AW-F, Chan Y-W. Mol. Genet. Metab 2002;75:91. [PubMed: 11825068]
5. Kisker C, Schindelin H, Pacheco A, Wehbi WA, Garrett RM, Rajagopalan KV, Enemark JH, Rees DC. Cell 1997;91:973. [PubMed: 9428520]
6. Astashkin AV, Johnson-Winters K, Klein EL, Byrne RS, Hille R, Raitsimring AM, Enemark JH. J. Am. Chem. Soc 2007;129:14800. [PubMed: 17983221]
7. Brody MS, Hille R. Biochim. Biophys. Acta 1995;1253:133. [PubMed: 8519792]
8. Hille R. Chem. Rev 1996;96:2757. [PubMed: 11848841]
9. Feng C, Wilson HL, Hurley JK, Hazzard JT, Tollin G, Rajagopalan KV, Enemark JH. Biochemistry 2003;42:12235. [PubMed: 14567685]
10. Karakas E, Wilson HL, Graf TN, Xiang S, Jaramillo-Busquets S, Rajagopalan KV, Kisker C. J. Biol. Chem 2005;280:33506. [PubMed: 16048997]
11. Field SJ, Thornton NP, Anderson LJ, Gates AJ, Reilly A, Jepson BJN, Richardson DJ, George SJ, Cheesman MR, Butt JN. Dalton Trans 2005:3580. [PubMed: 16234941]
12. Turner N, Ballard AL, Bray RC, Ferguson S. Biochem. J 1988;252:925. [PubMed: 2844161]
13. Doonan CJ, Wilson HL, Rajagopalan KV, Garrett RM, Bennett B, Prince RC, George GN. J. Am. Chem. Soc 2007;129:9421. [PubMed: 17608478]

14. Kappler U, Bailey S. J. Biol. Chem 2005;280:24999. [PubMed: 15863498]
15. Schrader N, Fischer K, Theis K, Mendel RR, Schwarz G, Kisker C. Structure 2003;11:1251. [PubMed: 14527393]
16. Enemark JH, Astashkin AV, Raitsimring AM. Dalton Trans 2006:3501. [PubMed: 16855750]
17. Raitsimring AM, Astashkin AV, Feng CJ, Wilson HL, Rajagopalan KV, Enemark JH. Inorg. Chim. Acta 2008;361:941.
18. Astashkin AV, Hood BL, Feng CJ, Hille R, Mendel RR, Raitsimring AM, Enemark JH. Biochemistry 2005;44:13274. [PubMed: 16201753]
19. Pacheco A, Basu P, Borbat P, Raitsimring AM, Enemark JH. Inorg. Chem 1996;35:7001. [PubMed: 11666879]
20. George GN, Garrett RM, Graf T, Prince RC, Rajagopalan KV. J. Am. Chem. Soc 1998;120:4522.
21. Temple CA, Graf TN, Rajagopalan KV. Arch. Biochem. Biophys 2000;383:281. [PubMed: 11185564]
22. Glasoe PK, Long FA. J. Phys. Chem 1960;64:188.
23. Dowerah D, Spence JT, Singh R, Wedd AG, Wilson GL, Farchione F, Enemark JH, Kristofzski J, Bruck M. J. Am. Chem. Soc 1987;109:5655.
24. http://quiz2.chem.arizona.edu/epr
25. Astashkin AV, Enemark JH, Raitsimring AM. Concepts Magn. Reson., Part B 2006;29B:125.
26. Bray, RC. Biological Magnetic Resonance. Berliner, LJ.; Reuben, J., editors. Vol. 2. Plenum Press; New York: 1980. p. 45
27. Lamy MT, Gutteridge S, Bray RC. Biochem. J 1980;185:397. [PubMed: 6249254]
28. Bray RC, Gutteridge S, Lamy MT, Wilkinson T. Biochem. J 1983;211:227. [PubMed: 6307274]
29. Astashkin AV, Raitsimring AM, Feng C, Johnson JL, Rajagopalan KV, Enemark JH. Appl. Magn. Reson 2002;22:421.
30. Codd R, Astashkin AV, Pacheco A, Raitsimring AM, Enemark JH. J. Biol. Inorg. Chem 2002;7:338. [PubMed: 11935358]
31. Astashkin AV, Mader ML, Pacheco A, Enemark JH, Raitsimring AM. J. Am. Chem. Soc 2000;122:5294. After the publication of this paper, we have often encountered a misinterpretation of our results [18,31–33] as indicating a free rotation of the OH ligand around the Mo—O bond. Therefore, we stress here that this idea was never entertained by us because at the measurement temperature of~20 K dynamic rotation is not plausible. Rather, our results are based upon a static structural distribution of the orientations of the OH ligand. The word“rotation”(around the Mo—O bond) has entered that description to specify the geometrical transformation relating all the different structural conformations.
32. Astashkin AV, Raitsimring AM. J. Magn. Reson 2000;143:280. [PubMed: 10729254]
33. Raitsimring AM, Pacheco A, Enemark JH. J. Am. Chem. Soc 1998;120:11263.
34. Raitsimring AM, Kappler U, Feng C, Astashkin AV, Enemark JH. Inorg. Chem 2005;44:7283. [PubMed: 16212344]
35. Astashkin AV, Kawamori A, Kodera Y, Kuroiwa S, Akabori K. J. Chem. Phys 1995;102:5583.
36. Doan PE, Hoffman BM. Chem. Phys. Lett 1997;269:208.
37. Mims WB. Proc. R. Soc. London A 1965;283:452.
38. Astashkin AV, Feng C, Raitsimring AM, Enemark JH. J. Am. Chem. Soc 2005;127:502. [PubMed: 15643856]
39. Astashkin AV, Neese F, Raitsimring AM, Cooney JJA, Bultman E, Enemark JH. J. Am. Chem. Soc 2005;127:16713. [PubMed: 16305262]
40. Gutteridge S, Lamy MT, Bray RC. Biochem. J 1980;191:285. [PubMed: 6258584]
41. Bray RC, Gutteridge S. Biochemistry 1982;21:5992. [PubMed: 6295449]
42. Gutteridge S, Malthouse JPG, Bray RC. J. Inorg. Biochem 1979;11:355.
43. Morpeth FF, George GN, Bray RC. Biochem. J 1984;220:235. [PubMed: 6331408]
44. Cramer SP, Johnson JL, Rajagopalan KV, Sorrell TN. Biochem. Biophys. Res. Commun 1979;91:434. [PubMed: 229850]
45. Van Doorslaer S, Schweiger A. Chem. Phys. Lett 1997;281:297.

46. Enemark JH, Astashkin AV, Raitsimring AM, Johnson-Winters K, Klein EL, Byrne RS, Hille R, Wilson HL, Rajagopalan KV. J. Biol. Inorg. Chem 2007;12(Suppl 1):S63.

47. Feng C, Wilson HL, Hurley JK, Hazzard JT, Tollin G, Rajagopalan KV, Enemark JH. J. Biol. Chem 2003;278:2913. [PubMed: 12424234]

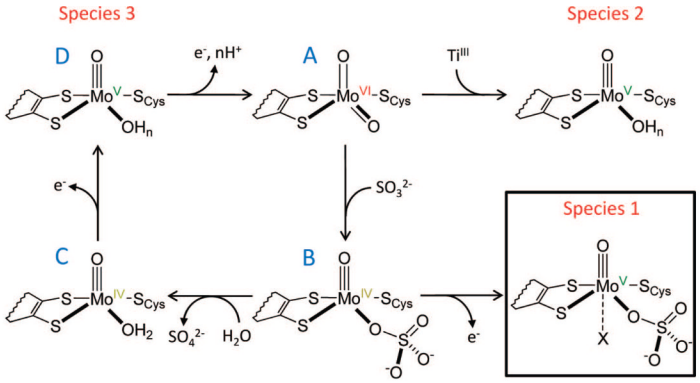

[a] Species 1, a "blocked" form with bound sulfate, is formed exclusively at pH ≤ 6 and is the subject of this study. Species 2, formed by reduction with Ti(III) at low pH, is also the major Mo(V) species produced by sulfite reduction at pH ~7.2.[13] Species 3 is formed at high pH and is analogous to the "primary" high pH form observed in wild type SO.

Scheme 1.

Proposed transformations of the Mo active site for the fatal R160Q mutant of human SO.[a]

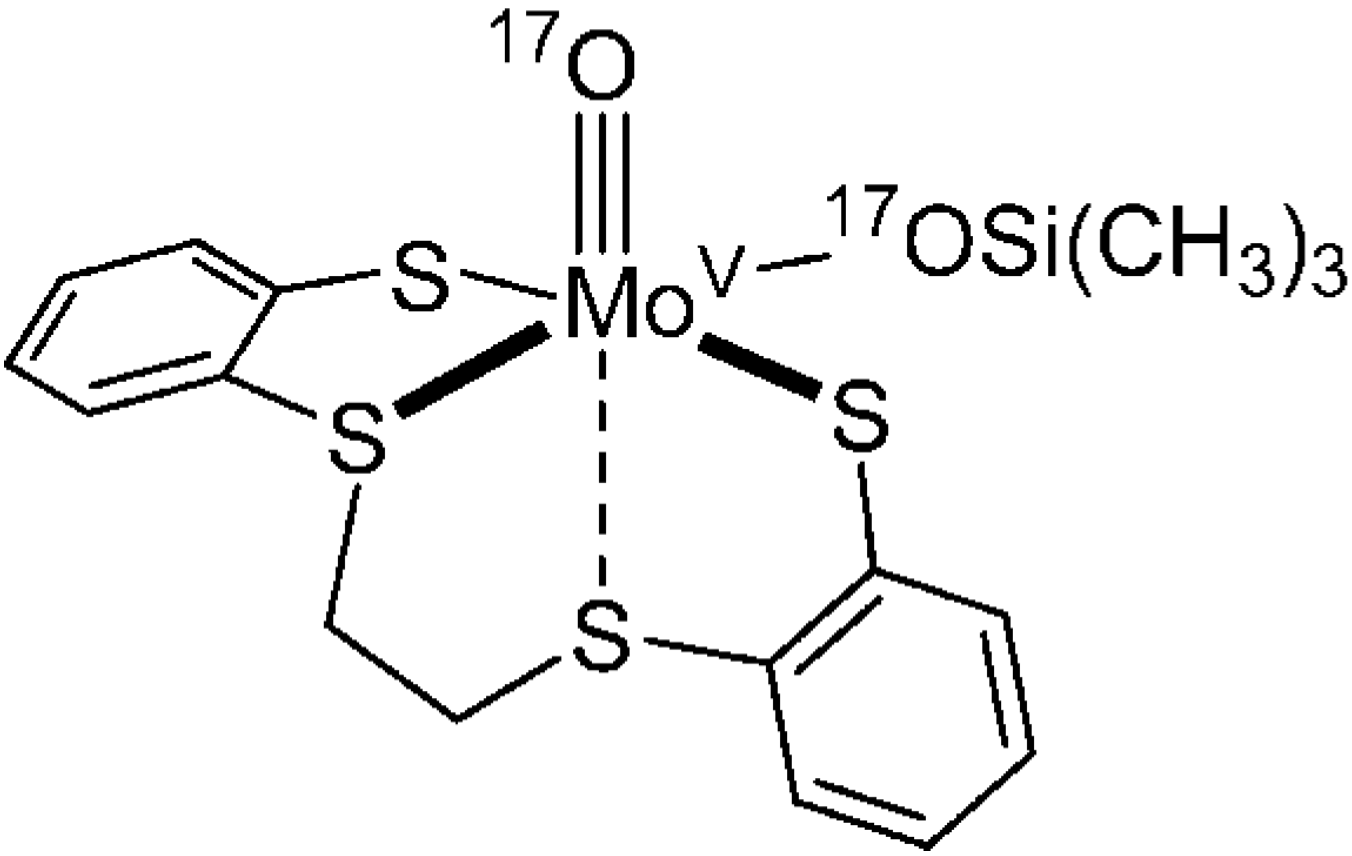

Chart 1.
The model complex (dttd)Mo^{17}O(^{17}Otms)

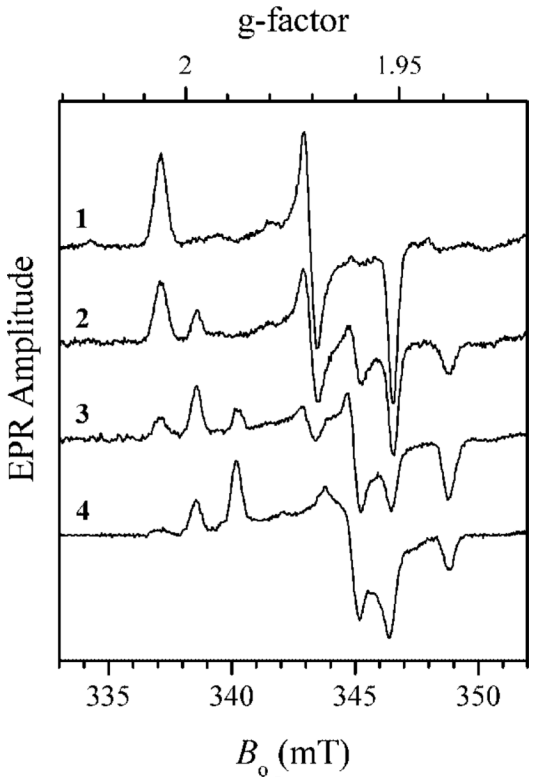

Figure 1.
Traces 1–4, CW EPR spectra of sulfite-reduced R160Q SO at pH 6.0, 7.2, 8.1, and 8.9, respectively. Experimental conditions: ν_{mw} = 9.465 GHz, mw power, 0.2 mW; modulation amplitude, 0.4 mT; temperature, 77 K.

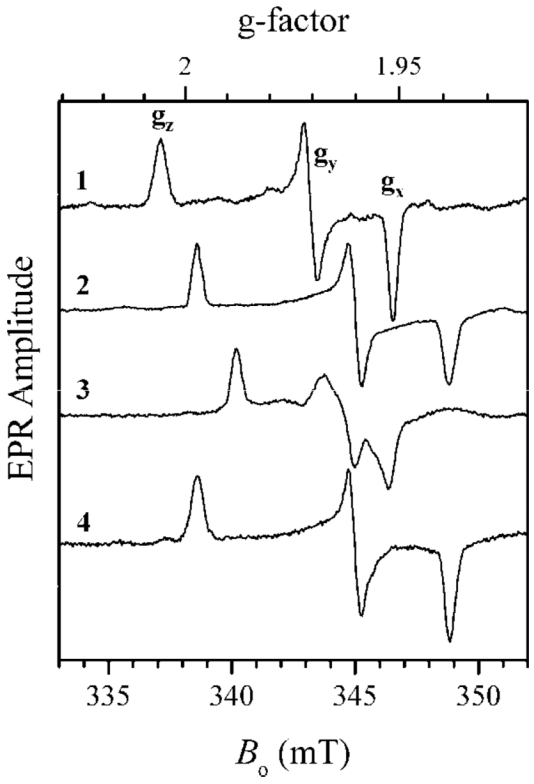

Figure 2.

Trace 1, CW EPR spectrum of sulfite-reduced R160Q SO at pH 6.0 (same as trace 1 in Figure 1). Traces 2 and 3, individual spectra contributing (along with spectrum 1) to the CW EPR spectra of sulfite-reduced R160Q SO at higher pH (see traces 2–4 in Figure 1). Trace 4, CW EPR spectrum of Ti(III) citrate-reduced R160Q SO at pH 7.0. Experimental conditions are the same as those for Figure 1.

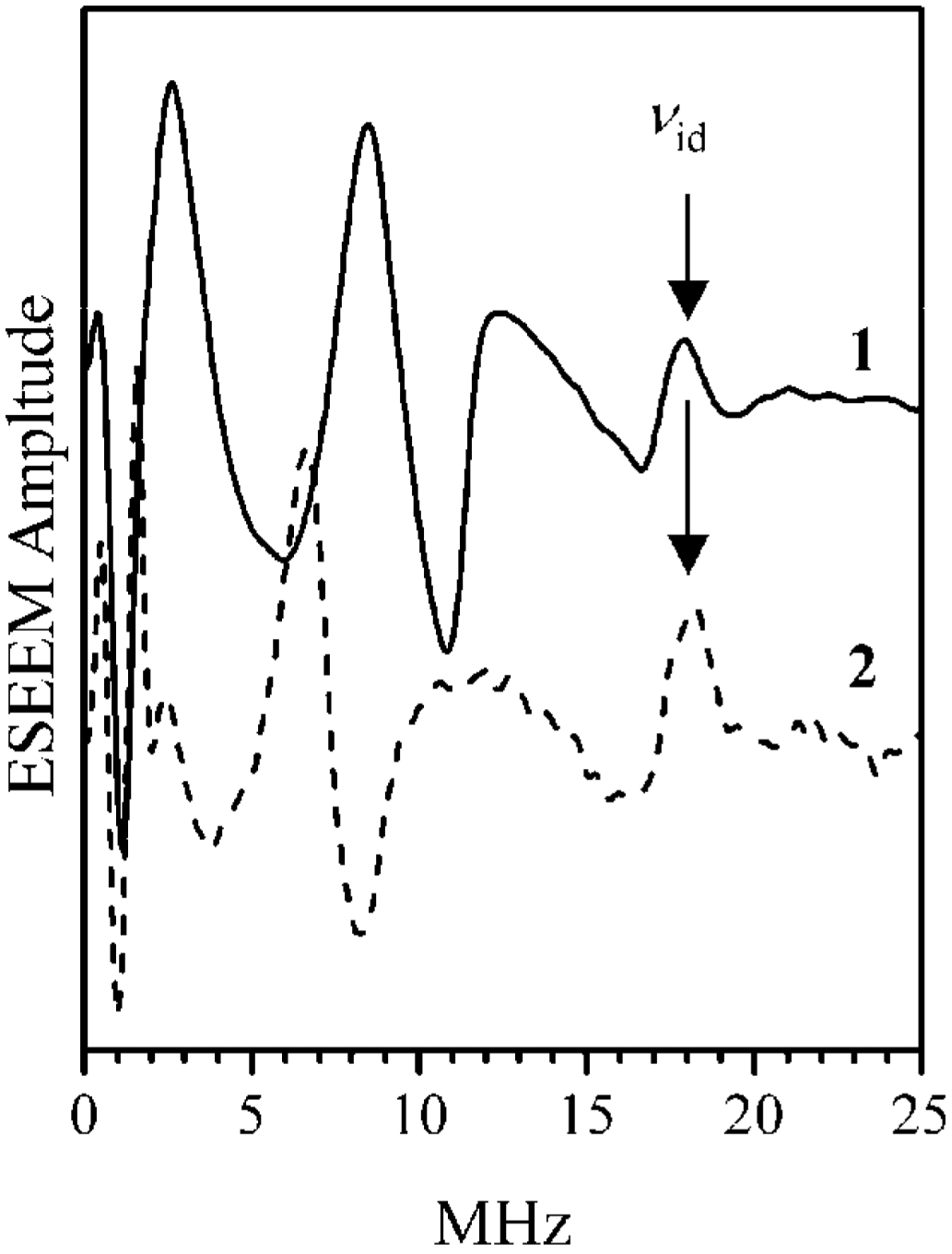

Figure 3.

Traces 1 and 2 are, respectively, K_a-band and K_u-band two-pulse ESEEM spectra (cosine FT) of *lpH* ^{33}S-R160Q SO (Species 1) obtained at g_z. Experimental conditions for trace 1: ν_{mw} = 29.472 GHz; B_o = 1050.8 mT; mw pulses, 2 × 13 ns. Experimental conditions for trace 2: ν_{mw} = 17.269 GHz; B_o = 618 mT; mw pulses, 2 × 10 ns. The temperature was 20 K for both traces.

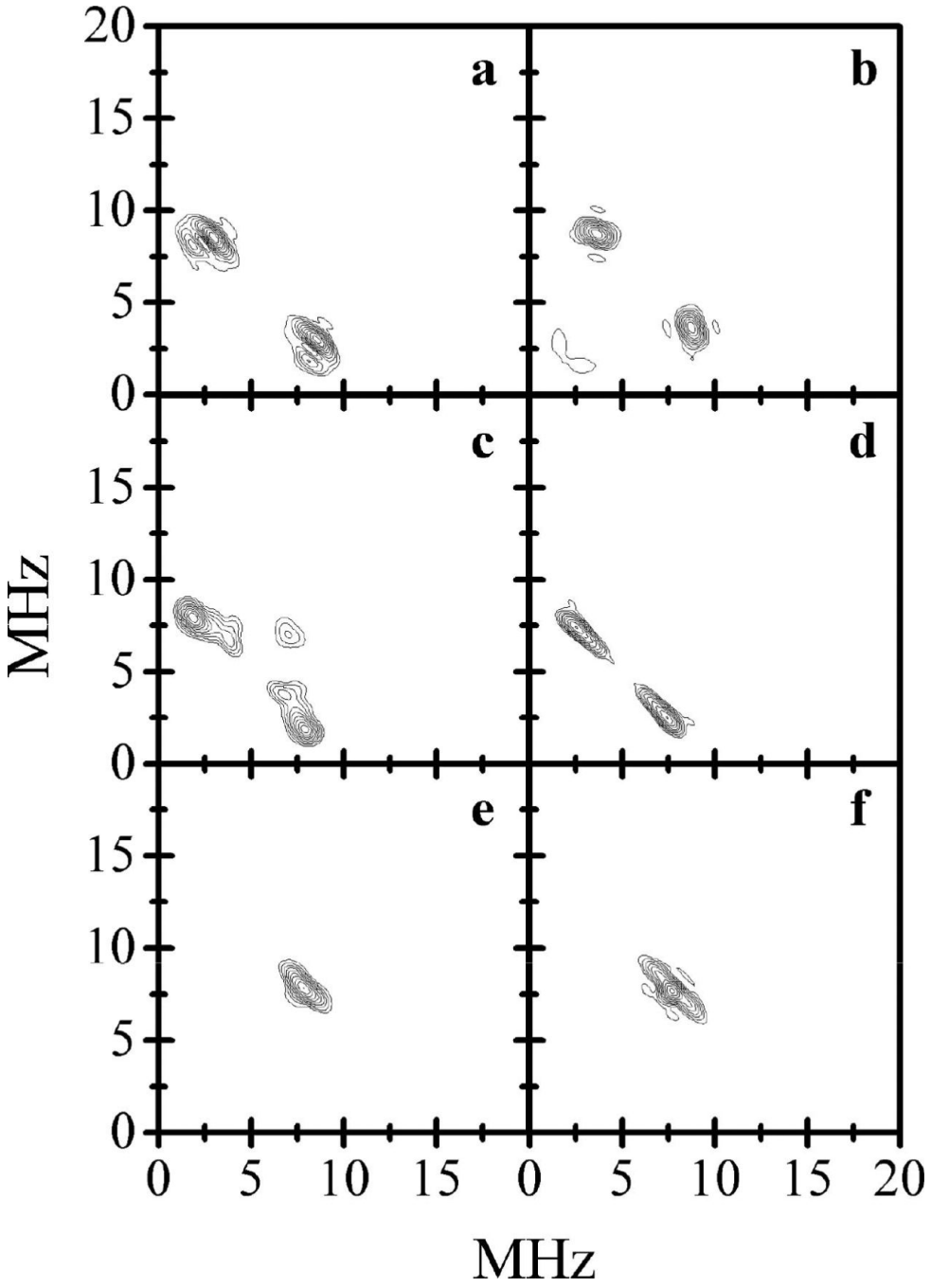

Figure 4.

Panels a, c, and e, the (++) quadrants of the HYSCORE spectra of ^{33}S-R160Q SO (Species 1) obtained at the g_z, g_y, and g_x EPR turning points, respectively (B_o = 1060.8, 1078.8, and 1088.6 mT, respectively). The spectra shown represent sums of the spectra obtained at time intervals between the first and second mw pulses τ = 170 and 200 ns. Other experimental conditions: ν_{mw} = 29.650 GHz; mw pulses, 11, 11, 21, and 11 ns; temperature, 20 K. Panels b, d, and f, simulated HYSCORE spectra for g_z, g_y, and g_x at the EPR turning points, respectively. Simulation parameters: a_{iso} = 2.1 MHz, anisotropic *hfi* tensor in the principal axes system, (T_{11}, T_{22}, T_{33}) = (–4.1, 2.5, 1.6) MHz; e^2Qq/h = 36 MHz; η = 0.2; Euler angles for the orientation of the *hfi* tensor in the *g*-frame: φ_h = 20°, θ_h = 10°, Ψ_h = 20°; Euler angles for the orientation

of the *nqi* tensor with respect to the *g*-frame: $\varphi_q = 90°$, $\theta_q = 90°$, $\Psi_q = 0°$. The simulated spectra (as experimental ones) represent sums of the spectra calculated for $\tau = 170$ and 200 ns.

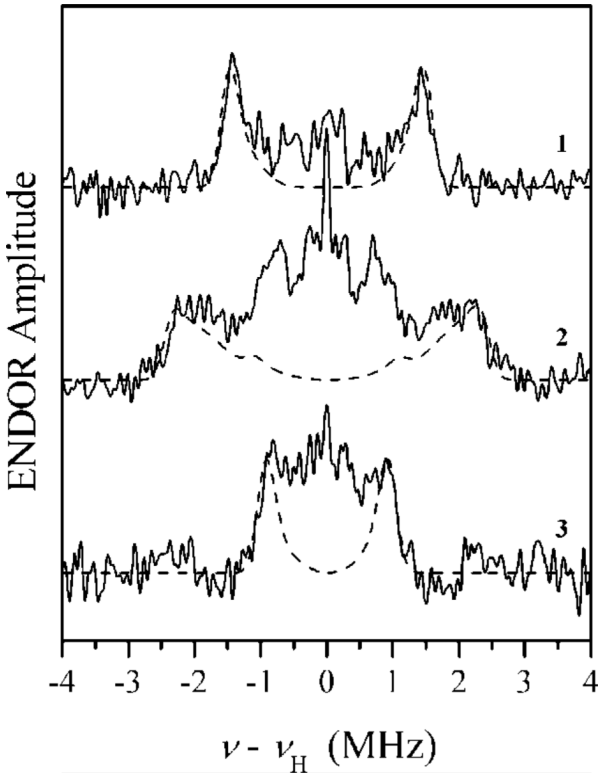

Figure 5.

Solid traces, ^{1}H ENDOR spectra at the EPR turning points (traces 1–3) obtained as a difference between the Re-Mims ^{1}H ENDOR spectra recorded for Species 1 of R160Q in H_2O and D_2O. Experimental conditions: B_o = 1051.3 mT (g_z), 1069.4 mT (g_y) and 1079.1 mT (g_x) for traces 1, 2, and 3, respectively; ν_{mw} = 29.470 GHz; mw pulses, 3 × 14 ns + 25 ns; time interval between the first and second mw pulses, τ = 80 ns; time interval between the second and third mw pulses, T = 30 μs; time interval between the third and fourth (refocusing) mw pulses, τ' = 380 ns; RF pulse length, 20 μs; temperature, 20 K. Dashed lines, numerical simulations for $\langle a_{iso} \rangle$ = 0; Δa_{iso} = 0.5 MHz; **T** = (–3.0, –1.9, 4.9) MHz; (φ_h,θ_h,Ψ_h) = (75°,80°,0°).

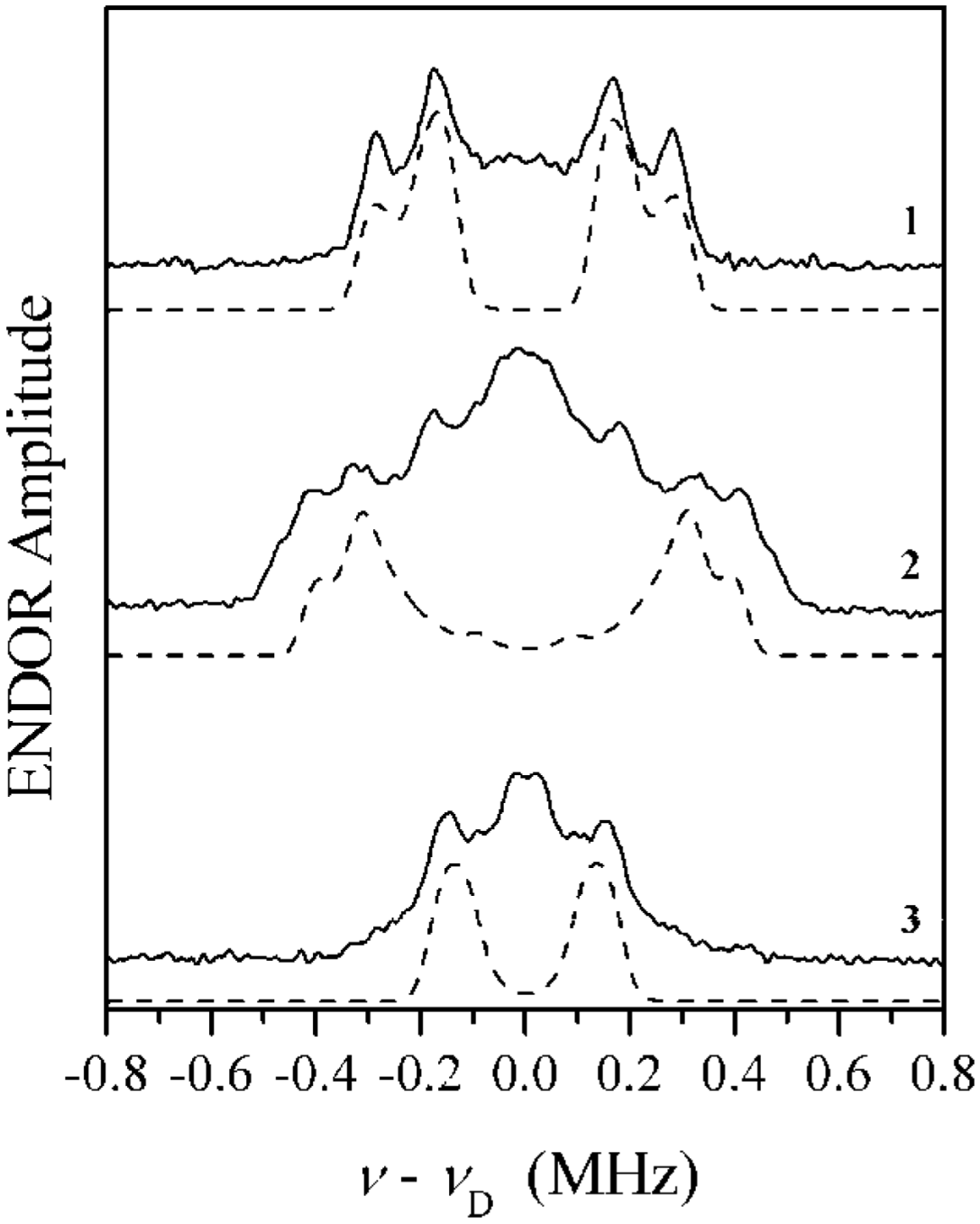

Figure 6.

Solid traces, Mims ^{2}H ENDOR spectra for Species 1 of R160Q in D_2O obtained at the EPR turning points. Experimental conditions: B_o = 1056.5 mT (g_z), 1074.6 mT (g_y) and 1084.3 mT (g_x) for traces 1, 2, and 3, respectively; ν_{mw} = 29.613 GHz; mw pulses, 3 × 14 ns; time interval between the first and second mw pulses, τ = 400 ns; time interval between the second and third mw pulses, T = 32 μs; RF pulse length, 26 μs; temperature, 20 K. Dashed traces, simulated numerically with parameters: $\langle a_{iso} \rangle$ = 0; Δa_{iso} = 0.077 MHz; **T** = (–0.46, –0.29, 0.75) MHz; (φ_h, θ_h, Ψ_h) = (75°, 80°, 0°), e^2Qq/h = 0.2 MHz; η = 0; (φ_q, θ_q, Ψ_q) = (30°, –45°, 0°).

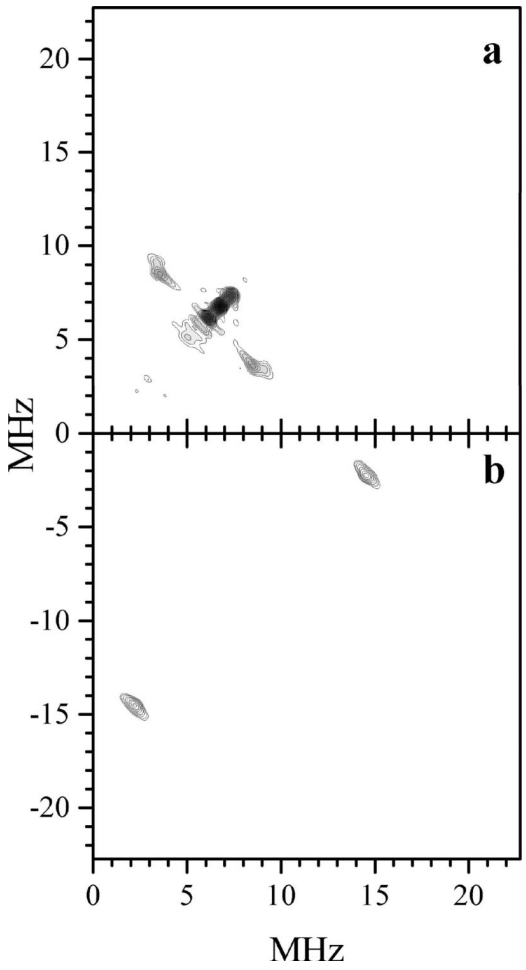

Figure 7.
HYSCORE spectrum of Species 1 in ^{17}O-R160Q SO showing the lines of oxo-^{17}O in (++) quadrant and equatorial ^{17}O in (+–) quadrant. Experimental conditions: ν_{mw} = 29.530 GHz; B_0 = 1070 mT (g_y); mw pulses, 10, 10, 20, and 10 ns; time interval between the first and second mw pulses, τ = 180 ns; temperature, 20 K.

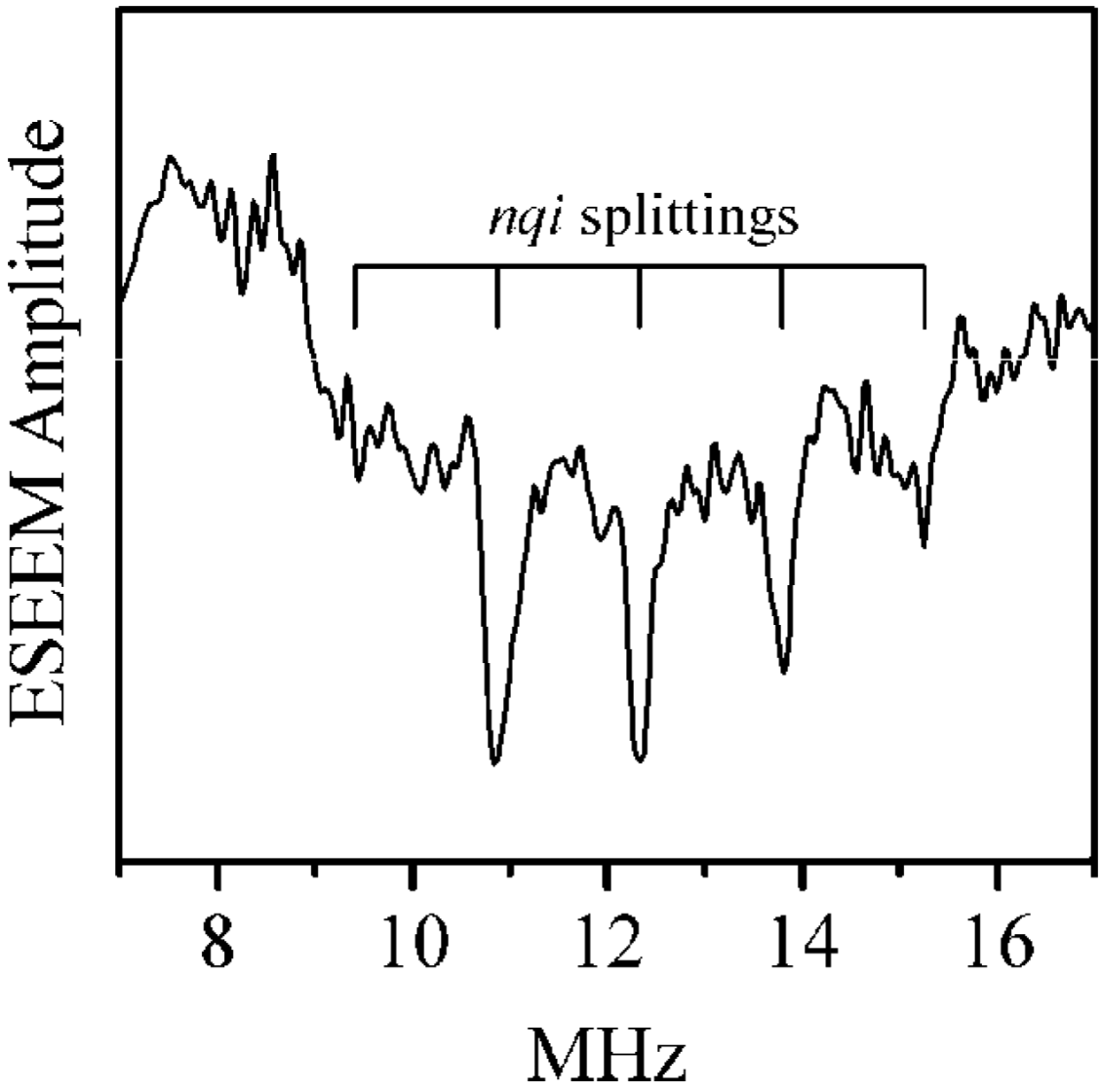

Figure 8.

^{17}O sum combination line region of τ-integrated four-pulse ESEEM spectrum (cosine FT) of Species 1 of ^{17}O-R160Q SO obtained at g_z. Experimental conditions: ν_{mw} = 29.530 GHz; B_o = 1052 mT; mw pulses, 10, 10, 20, and 10 ns; starting time interval between the first and second mw pulses, τ = 180 ns; temperature, 20 K.

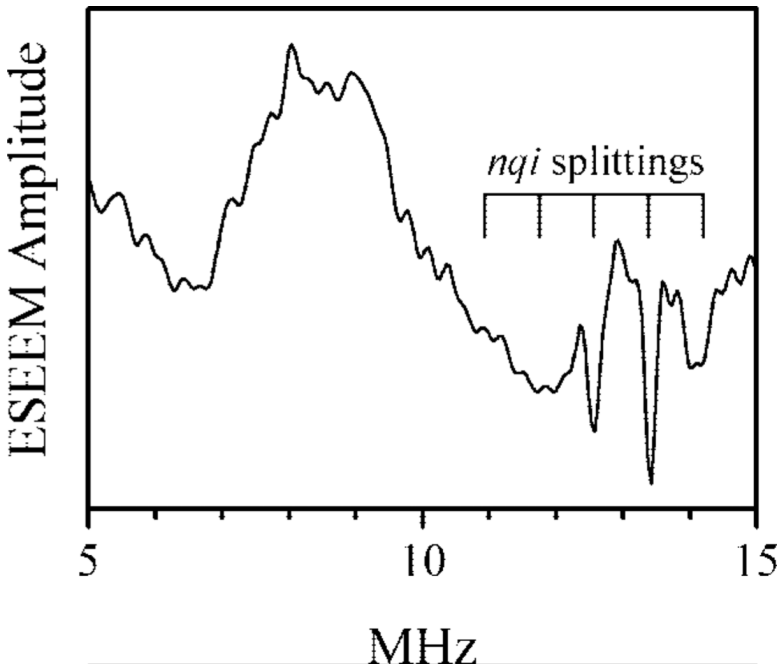

Figure 9.

^{17}O sum combination line region of τ-integrated four-pulse ESEEM spectrum (cosine FT) of (dttd)Mo^{17}O(^{17}Otms) obtained at g_z. Experimental conditions: ν_{mw} = 29.804 GHz; B_o = 1081.5 mT; mw pulses, 18, 18, 36, and 18 ns; starting time interval between the first and second mw pulses, τ = 180 ns; temperature, 20 K.

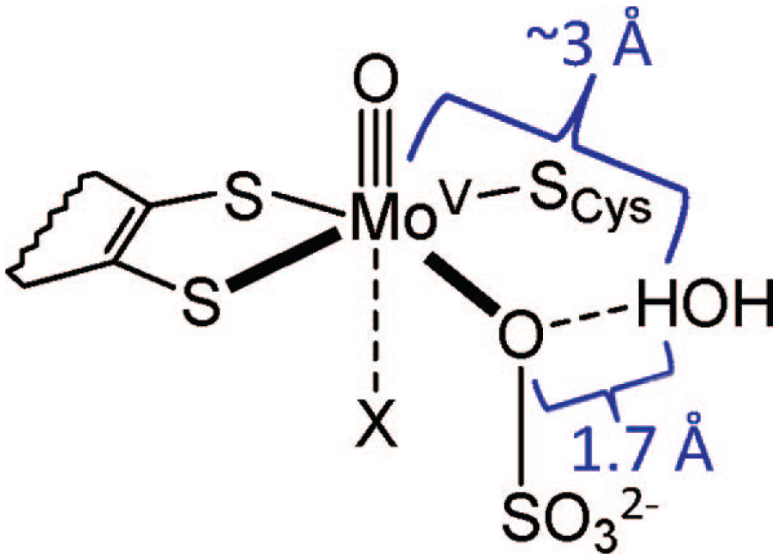

Figure 10.
Envisioned structure of the Mo center of Species 1 of R160Q SO resulting from the pulsed EPR experiments. “X” is a putative axial ligand coordinated *trans* to the oxo ligand.

Table 1

Principal *g*-Values of EPR-Active Mo(V) Species Observed in R160Q SO in Comparison with Those Found in SO Enzymes from Other Sources

Mo(V) species	g_z	g_y	g_x	reference
Species 1	2.006	1.971	1.951	this work
(observed at low pH ~ 6.0)	2.0061	1.9708	1.9514	13
Species 2	1.998	1.961	1.939	this work
(observed at higher pH)	1.9978	1.9604	1.9391	13
Species 3	1.988	1.964	1.953	this work
(observed at higher pH)	1.9875	1.9636	1.9526	13
low-pH form of SO (chicken)	2.0037	1.972	1.9658	26, 27
high-pH form of SO (chicken)	1.9872	1.9641	1.9531	26, 27
“blocked” form of At-SO	2.005	1.974	1.963	6, 18

Table 2

Sets[a] of *hfi* Constants **A** = (A_x, A_y, A_z) Estimated from Analysis of HYSCORE Spectra at g_x, g_y, and g_z, and the Isotropic *hfi* Constants a_{iso} and the Anisotropic *hfi* Constants **T** = (T_x, T_y, T_z) Estimated from **A**

set	(A_x, A_y, A_z) [MHz]	a_{iso} [MHz]	(T_x, T_y, T_z) [MHz]
I	±(0, 4.5, 3.4)	±2.63	±(–2.63, 1.87, 0.77)
II	±(0, 4.5, –3.4)	±0.37	±(–0.37, 4.13, –3.77)

[a] The sets differ by the choice of relative signs of different components of **A**.